

CARE: Contrastive Alignment for ADL Recognition from Event-Triggered Sensor Streams

Junhao Zhao*

*Electrical and Computer Engineering
University of Maryland, College Park
Maryland, USA
jzhao121@umd.edu*

Zishuai Liu

*School of Computing
University of Georgia
Athens, USA
zishuai.liu@uga.edu*

Ruili Fang

*School of Computing
University of Georgia
Athens, USA
ruili.fang@uga.edu*

Jin Lu

*School of Computing
University of Georgia
Athens, USA
jin.lu@uga.edu*

Linghan Zhang

*Human Interaction Technology
Eindhoven University of Technology
Eindhoven, Netherlands
l.zhang1@tue.nl*

Fei Dou†

*School of Computing
University of Georgia
Athens, USA
fei.dou@uga.edu*

Abstract—The recognition of Activities of Daily Living (ADLs) from event-triggered ambient sensors is an essential task in Ambient Assisted Living, yet existing methods remain constrained by representation-level limitations. Sequence-based approaches preserve temporal order of sensor activations but are sensitive to noise and lack spatial awareness, while image-based approaches capture global patterns and implicit spatial correlations but compress fine-grained temporal dynamics and distort sensor layouts. Naïve fusion (e.g., feature concatenation) fail to enforce alignment between sequence- and image-based representation views, underutilizing their complementary strengths. We propose Contrastive Alignment for ADL Recognition from Event-Triggered Sensor Streams (CARE), an end-to-end framework that jointly optimizes representation learning via Sequence–Image Contrastive Alignment (SICA) and classification via cross-entropy, ensuring both cross-representation alignment and task-specific discriminability. CARE integrates (i) time-aware, noise-resilient sequence encoding with (ii) spatially-informed and frequency-sensitive image representations, and employs (iii) a joint contrastive-classification objective for end-to-end learning of aligned and discriminative embeddings. Evaluated on three CASAS datasets, CARE achieves state-of-the-art performance (89.8% on Milan, 88.9% on Cairo, and 73.3% on Kyoto7) and demonstrates robustness to sensor malfunctions and layout variability, highlighting its potential for reliable ADL recognition in smart homes.

Index Terms—ambient intelligence, activities of daily living, event-triggered time series, contrastive learning

I. INTRODUCTION

Global increases in life expectancy are leading to aging societies, with a rising number of older adults who require continuous support from healthcare providers and their family members [30]. However, given the critical shortage of healthcare personnel, it is essential to support older adults in maintaining independence for as long as possible. [16]. An essential component of independent living is the ability to perform Activities of Daily Living (ADLs)—such as toileting, dressing, feeding, and cooking—that directly determine an

individual’s quality of life. These functional abilities often decline with aging, and can be further deteriorated by aging-related chronic conditions [32].

Ambient Assisted Living (AAL) technologies have emerged to support ADL performance, encompassing systems for activity recognition, anomaly detection, and personalized prompting. Among these, *ambient sensor-based systems* are especially attractive for AAL, as they provide unobtrusive and privacy-preserving monitoring without the discomfort of wearables or the intrusiveness of cameras [15]. Embedded in home environments, ambient sensors offer passive, continuous, and cost-effective monitoring of motion, door usage, and environmental states, enabling scalable deployment in real-world homes [12], [13].

Despite these advantages, ADL recognition from ambient sensors is inherently challenging. Different from continuously sampled wearable sensor signals, ambient sensors generate *event-triggered time series* that are sparse, irregular, and noisy: motion sensors activate only when residents pass by, door sensors only when opened or closed. Moreover, older adults often perform the same ADL with variations in order, speed, or completion, further complicating recognition [36]. To be reliable, recognition models must capture fine-grained temporal dynamics while also contextualizing spatial information across multiple sensors [2], [20], [21].

Two dominant strategies have been explored for encoding event-triggered ADL data. *Sequence-based methods* [4], [19], [22], [26] preserve event order to capture temporal dependencies, thereby modeling daily routines. However, they often ignore the absolute daily time context (e.g., morning vs. evening), are highly sensitive to noise, and lack explicit mechanisms for capturing spatial relationships among sensors. *Image-based methods* [18], [28], [35], in contrast, transform event streams into activity images, thereby leveraging global patterns and the implicit spatial correlations embedded in sensor indices. Yet, they suffer from distorted layouts introduced

*This work was done when the author was on exchange program at UGA.

†Corresponding author

TABLE I: Comparison of Encoding Methods for Event-Triggered Time Series in ADL Recognition.

Model	Input Repr.	Encoder	View	TimeResolution	PSI*	NR †	Fusion Strat.	LO ‡	End2End	Dataset
DeepCASAS [26]	Sequence	BiL	Uni-View	X	X	X	None	CE	Yes	CASAS
JointTemporalModel [19]	Sequence	BiL+1DCNN	Uni-View	Minute	X	✓	None	CE	Yes	Ordonez, Kastern
EmbeddingFCN [4]	Sequence	FCN	Uni-View	X	X	X	None	CE	Yes	CASAS
TCN [22]	Sequence	TCN	Uni-View	Hourly	X	X	None	CE	Yes	Self-conducted
BinaryCNN [35]	Image	CNN	Uni-View	X	X	X	None	CE	Yes	SH
DCNN [18]	Image	CNN	Uni-View	X	implicit	X	None	CE	Yes	CASAS
GreyDCNN [28]	Image	CNN	Uni-View	Local (Δt)	implicit	X	None	CE	Yes	Smart Home
GraphModel [31]	Graph	GNN	Uni-View	Unit Duration	implicit	Partial	None	CE	Partial	CASAS
TDOST [34]	Textual	BiL+SE†	Uni-View	Begin+Interval	description	X	None	CE	Partial	CASAS, Orange
Ours (CARE)	Seq+Img	BiL+Res	Cross-View	Hour-binned	✓	✓	ContraAlign	SICA+CE	Yes	CASAS

*PSI: Physical Spatial Information, †NR: Noise Robust, ‡LO: Learning Objective, † SE: Sentence Encoder, BiL: BiLSTM, CE: Cross-Entropy.

by artificial 1D indexing, reduced temporal resolution that obscures fine-grained dynamics, and the neglect of sensor activation frequency as a potentially discriminative feature.

These limitations highlight a major gap: existing methods focus exclusively on either sequence or image encodings, treating temporal and spatial cues in isolation, and missing the opportunity to exploit their natural complementarity. Prior work has explored simple fusion strategies—such as feature concatenation or late fusion. While naïve fusion strategy (simple concatenation) could, in principle, combine both views, it ignores cross-view interactions and lacks explicit constraints to ensure that both representation views are effectively utilized, limiting its ability to fully leverage complementary information. To overcome this, we argue for a unified framework that can jointly leverage both perspectives within a shared latent space.

To this end, we propose **CARE** (A Contrastive Alignment Framework for ADL Recognition from Event-Triggered Sensor Streams), an end-to-end framework that unifies sequence- and image-based representations through supervised contrastive alignment and joint classification learning. At its core, CARE introduces **SICA** (Sequence-Image Contrastive Alignment), a supervised contrastive mechanism that aligns embeddings from the two representation views in a shared latent space. By enforcing both intra- and cross-view consistency, SICA produces richer, noise-resilient, and class-discriminative representations. By coupling alignment and classification within one optimization stage, CARE avoids the common two-step pipeline of representation pretraining followed by classifier training, thereby producing deployment-ready models that balance robustness, efficiency, and interpretability.

The main contributions of this work are threefold:

- *Robust temporal encoding.* We design a time-aware and noise-resilient sequence encoding method that preserves global daily context while mitigating impact of spurious sensor firings, addressing the limitations of prior order-only encodings.
- *Spatially-informed image representation.* We propose a dual-perspective image representation that integrates temporal dynamics with floorplan-based spatial cues and frequency-sensitive transitions, enabling richer and more interpretable activity patterns.

- *cross-view contrastive alignment (SICA).* We introduce a supervised contrastive alignment objective that unifies sequence- and image-based embeddings in a shared latent space, enforcing view-invariant and class-consistent representations.
- *Unified end-to-end framework (CARE).* Building on SICA, we develop CARE, a one-stage framework that jointly optimizes representation learning and classification, eliminating multi-stage retraining and improving deployment readiness for real-world ADL systems.

II. RELATED WORK

The integration of ambient sensors into assistive living technologies has shown strong potential to promote independent living and enable early detection of health deterioration [27]. Research has demonstrated that ambient sensor data, when analyzed with advanced machine learning techniques, can effectively classify and predict ADLs with high accuracy [1]. Ambient sensor-based systems are especially attractive for AAL because they are unobtrusive, cost-effective, and scalable, offering continuous monitoring of motion, door usage, and environmental states in naturalistic homes [12], [13]. Moreover, they align with broader trends toward privacy-preserving monitoring, respecting autonomy while enabling timely health alerts [17]. However, the event-triggered nature of such data makes ADL recognition inherently challenging: signals are sparse, irregular, and noisy, and older adults often perform the same activity with variations in order, speed, or completion [36]. These characteristics underscore the need for robust representation learning methods that can jointly capture fine-grained temporal dynamics and cross-sensor spatial context [2], [20], [21].

Table I summarizes representative encoding strategies of event-triggered sensor data for ADL recognition. Below, we review four main lines of work.

Sequence-based Deep Learning Methods. A widely adopted approach is to model event-triggered sensor streams as temporal sequences, leveraging deep sequence models to capture event order and temporal dependencies. LSTM and its variants (e.g., Bi-LSTM) have been applied extensively for activity recognition [26], [29], with extensions that integrate convolutional layers to enhance local feature extraction [19]. Other architectures, such as Fully Convolutional Networks (FCN) [4] and Temporal Convolutional Networks (TCN) [22] have also

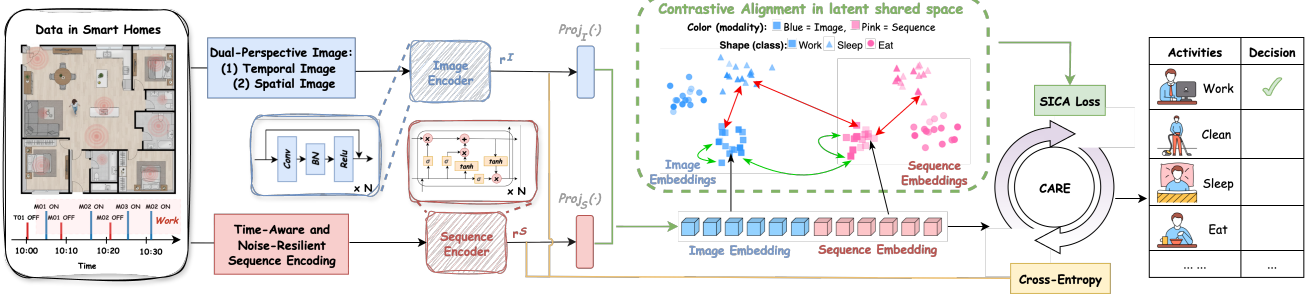


Fig. 1: Contrastive Alignment for ADL Recognition from Event-Triggered Sensor Streams (CARE) Framework.

been explored. These models, originally popularized in domains like natural language processing, enable the learning of hierarchical dependencies and activity flow from sensor event sequences. While effective at capturing the temporal flow of activities, these methods often *ignore absolute daily time context*, which is crucial for distinguishing activities that share similar local patterns but occur at different times (e.g., sleeping at night vs. napping in the afternoon). Moreover, sequence-only methods are highly sensitive to noise and outliers [3], and they fail to explicitly capture cross-sensor spatial relationships that are key to disambiguating similar activities.

Image-Based Encoding Approaches. An alternative line of work transforms event streams into images and applies convolutional encoders. BinaryCNN [35], DCNN [18] and Grey-DCNN [28] map sensor activations into binary or grayscale activity images, allowing CNNs to exploit global structures and long-range correlations of time series. These approaches are generally more robust to noise than sequence encoders, since image representations smooth over missing or spurious events. However, several limitations remain: (i) the commonly used 1D sensor indexing distorts the true 2D spatial layout, placing unrelated sensors adjacently and losing room-level semantics; (ii) temporal details are compressed into a single axis or pixel intensity, weakening fine-grained activity dynamics; and (iii) all sensor activations are treated equally, overlooking activation frequency as a discriminative cue.

Other Input Representations. Graph-based approaches [31] represent sensor activations as nodes and transitions as edges, enabling explicit modeling of cross-sensor relationships. While effective on certain datasets, such models are computationally expensive due to the repeated graph construction and inference iterations, which limit their scalability in real-world deployments. More recently, textual encodings have emerged: Jüttner et al. [23] applied GPT-4 to infer ADLs and detect anomalies in CASAS [12], while TDOST [34] tokenizes event sequences into words and leverages a pretrained sentence transformer followed by a BiLSTM and classifier. Notably, TDOST achieves state-of-the-art performance across several benchmarks without explicit temporal features, underscoring the potential of language-inspired representations. However, when this method plugin the time information into the words, the performance is not improved. This highlights an open question: how to exploit temporal information in non-traditional encodings like

text while preserving underlying activity patterns.

Contrastive Learning for ADL Recognition. Contrastive learning was initially designed to transform features so that similar samples are positioned close to each other in a transformed feature space [9]. While it has shown promise in domains such as vision and NLP [5], [8], [24], the adoption in ambient sensing remains limited [6], [7]. Existing ADL methods typically focus on single representation view or naïve fusion, where features from different views are concatenated and trained with cross-entropy loss. Such strategies lack explicit constraints to ensure that both views are effectively leveraged, and thus miss the opportunity to exploit cross-view complementarity. In contrast, our proposed method, the CARE framework, introduces a *supervised contrastive alignment* objective (SICA) that explicitly enforces consistency between sequence- and image-based embeddings in a shared latent space, addressing the limitations of prior methods and enabling more robust and discriminative ADL representations.

III. PROPOSED METHOD

Raw event-triggered sensor streams are first processed through a preprocessing pipeline, including segmentation, index mapping, padding, and signal normalization, to generate both image-based and sequence-based input representations. The sequence branch further processes the streams with temporal binning and frequency-based event filtering, followed by a recurrent encoder that captures temporal correlations and noise-resilient patterns. The image branch generates dual-perspective image representations consisting of a temporal image and a spatial image, which are encoded by convolutional networks to model spatial dependencies and global patterns. The encoders' outputs are projected into a shared latent space, where a contrastive alignment objective enforces view-invariant, class-consistent embeddings. Along with a cross-entropy classification head, the proposed CARE framework (shown in Fig. 1) jointly performs robust representation learning and end-to-end activity recognition.

A. Time-Aware and Noise-Resilient Sequence Encoding

The aim of sequence encoding is to transform irregular and noisy event-triggered sensor streams into structured temporal representations that capture daily contextual routines while remaining robust to noise activations. Such representations

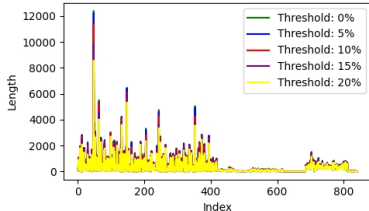


Fig. 2: Frequency-based Event Filtering on *Cairo*

should capture when activities are likely to occur and how sensor activations evolve over time, providing a foundation for downstream ADL recognition tasks.

Temporal Binning. A critical limitation of prior sequence encodings is their inability to handle temporal information. Existing methods [19], [22], [28], [31], [34] typically: (i) ignore timestamps entirely, discarding daily context; (ii) use inter-event intervals $\Delta t_i = t_i - t_{i-1}$, which capture local timing gaps but fail to reflect absolute daily temporal positioning; or (iii) combine inter-event intervals with activity begin times $(t_{\text{start}}, \Delta t_i)$, which anchors the sequence to its onset and preserves absolute time-of-day information at the activity level, but does not explicitly associate each sensor event with its own global timestamp. In contrast, our method assigns a coarse-grained temporal embedding to every event. For each raw time-of-day $t_i \in \mathbb{R}^+$, we compute

$$\tau_i = \left| \frac{t_i}{\Delta T} \right|,$$

where ΔT is a dataset-specific bin width (e.g., one hour for milan). This design ensures that each sensor event is embedded within the daily routine context (e.g., nighttime vs. midday) while suppressing minute-level fluctuations that are irrelevant for hour-level ADL recognition. The discretized index τ_i is then concatenated with sensor ID and signal state to form a event representation.

Frequency-based Event Filtering. Event-triggered sequences often contain accidental sensor activations that appear only once or a few times within an activity, yet unnecessarily inflate the sequence length and introduce noise. Naïve strategies, such as retaining all events, preserve irrelevant noise that can degrade recognition performance.

To achieve robustness, we adopt a frequency-based criterion to remove unreliable events. For an activity segment with n events, let f_j denote the activation count of sensor s_j . We normalize these counts as $\tilde{f}_j = \frac{f_j}{\max_k f_k}$, so that the most frequently activated sensor has $\tilde{f}_{j_{max}} = 1$. A sensor event is retained only if $\tilde{f}_j \geq \theta$, where $\theta \in (0, 1)$ is a dataset-specific threshold. As illustrated in Fig. 2, increasing the threshold θ progressively prunes low-frequency activations and shortens the sequences, trading off noise reduction against potential loss of rare but informative events.

Sequence Representation. To ensure consistency across heterogeneous sensor types, binary states (“ON/OPEN/PRESENT”) are mapped to 1 and others to 0, while continuous values such as temperature are

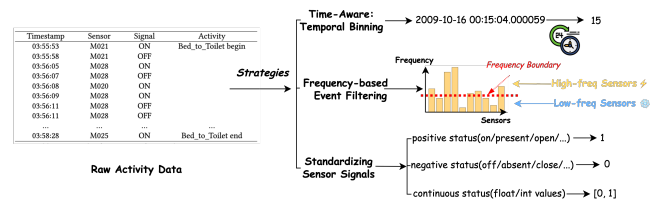


Fig. 3: Sequence Representation.

normalized to $[0, 1]$. Each activity segment is further padded or truncated to a fixed length L to enable batch processing. Each event is then represented by concatenating a one-hot encoding of its sensor ID, the temporal index τ_i , and the normalized signal state. The resulting enriched sequence is processed by a sequence encoder (e.g., LSTM) to generate temporal embeddings h_t that jointly capture sensor identity and contextualized temporal dependencies (Fig. 3).

B. Spatially-Informed and Frequency-Sensitive Image Representation

While sequence encoding captures temporal correlations, it is limited in modeling global structures across long sequences and inter-sensor relationships. An alternative approach is to transform event-triggered sequences into 2D activity images, allowing CNNs to exploit spatial patterns and long-range dependencies in a structured way.

Prior studies [18], [28] typically represent activities as binary or grayscale matrices, with the x -axis denoting event order and the y -axis denoting sensor IDs. This design has several advantages: it preserves the temporal order of events and, to some extent, encodes implicit spatial relations through the vertical sensor index. However, the spatial information is inaccurate, as the one-dimensional y -axis does not reflect the true two-dimensional floorplan. Sensors located in different rooms may be placed adjacently in the y -axis, leading to semantic confusion. Furthermore, such encodings treat all sensor activations equally and ignore their activation frequencies, failing to distinguish frequent transitions from sporadic noise.

To overcome these limitations, we propose a *dual-perspective image representation* consisting of a temporal image and a spatial image:

Temporal Image. For an activity segment with events $\{e_i\}_{i=1}^n$, where $e_i = (\tau_i, s_i, a_i)$ denotes temporal index, sensor ID, and normalized activation signal, we construct a temporal image I^{temp} such that $I^{\text{temp}}(x_i, y_i) = \phi(\text{idx}(\tau_i), s_i, a_i)$, where x_i corresponds to the event order (x_1 denotes the first timestamp, followed sequentially up to x_L after padding or truncation), y_i is the index of sensor s_i , and $\text{idx}(\tau_i)$ is the discretized time-bin index of timestamp. The mapping function $\phi(\cdot)$ integrates the time-bin index, sensor identity, and signal state into color channels (e.g., motion = blue, door = yellow, temperature = red). This representation highlights temporal dynamics while differentiating sensor modalities.

Spatial Image. Each sensor s_j is associated with normalized floorplan coordinates $(u_j, v_j) \in [0, 256]^2$. We construct a

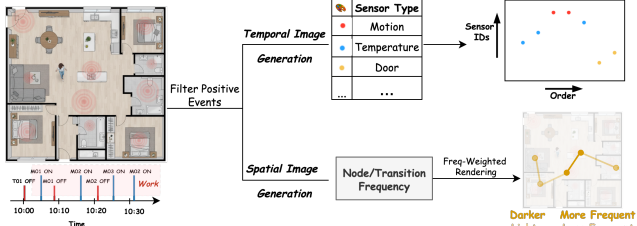


Fig. 4: Image Representation.

spatial image I^{spat} where nodes represent sensor positions and edges represent transitions between consecutive events. Nodes are rendered according to their activation frequency f_j (already defined in Sec. III-A), normalized by $\max_k f_k$, with darker colors indicating more frequently activated sensors. For edges, the transition from s_j to s_k is assigned weight

$$w_{jk} = c_{jk} / \max_{p,q} c_{pq},$$

where c_{jk} is the number of observed transitions between s_j and s_k in the segment, with darker edges denoting more frequent transitions. States such as “OFF”, “CLOSE”, and “ABSENT” are excluded to reduce clutter. This representation leverages the floorplan to embed spatial context and highlights recurrent patterns while suppressing sporadic noise.

Unified Image Representation. The temporal and spatial images are concatenated to form a composite image $I^{\text{comp}} = \text{concat}(I^{\text{temp}}, I^{\text{spat}})$, which jointly encodes temporal ordering, spatial configuration, and frequency awareness. The composite image is then processed by a CNN encoder to produce an embedding that is spatially-informed, frequency-sensitive, and robust to noise (Fig. 4).

C. Sequence–Image Contrastive Alignment (SICA)

Our goal is to unify the complementary strengths of the sequence- and image-domain streams by learning a shared latent space. The **sequence-domain stream** captures temporal dependencies explicitly. The **image-domain stream** emphasizes spatial relationships and frequency-sensitive patterns and also preserves implicit temporal order via event sequencing. These two perspectives are complementary and partially overlapping: one models fine-grained temporal dynamics, the other grounds activities in spatial context with implicit temporal correlations.

Without explicit interaction, however, training the two streams independently produces heterogeneous embeddings that cannot be directly fused, limiting cross-view synergy. A straightforward alternative is to concatenate the outputs of the two encoders and optimize a cross-entropy loss. While simple, this naive fusion does not explicitly enforce alignment between views: the classifier may overfit to the dominant stream, ignore complementary cues, and fail to enforce consistency between sequence- and image-based embeddings of the same activity.

To address these limitations, we propose **Sequence–Image Contrastive Alignment (SICA)**, which introduces a contrastive objective (i.e., the SICA loss) to explicitly align

sequence and image embeddings in one shared latent space. By pulling together cross-view embeddings of the same activity and pushing apart those of different activities, SICA enforces both cross-view alignment and class-level discriminability, enabling the model to fully exploit temporal and spatially grounded cues.

Projection Heads. To enable contrastive alignment across heterogeneous representation views, we introduce lightweight projection heads after both the sequence and image encoders. Each projection head is a single-layer MLP that maps view-specific encoder outputs into a shared latent space with matched dimensionality. This transformation ensures comparability across views and refines representations for contrastive learning.

Positive and Negative Pair Construction. Given a mini-batch B of activity segments, each input \mathbf{x}_i produces two embeddings after the projection heads: a sequence embedding \mathbf{z}_i^S and an image embedding \mathbf{z}_i^I . For each anchor embedding, positives are defined at two levels:

- *Intra-view positives*: embeddings from other samples of the same class within the same view of encoding (e.g., $(\mathbf{z}_i^S, \mathbf{z}_j^S)$ if $y_j = y_i$, where y represents class label.).
- *Cross-view positives*: the paired embedding of the same sample across domains (\mathbf{z}_i^S vs. \mathbf{z}_j^I), together with embeddings from the same class in the alternate view (e.g., $(\mathbf{z}_i^S, \mathbf{z}_j^I)$ if $y_j = y_i$).

All embeddings from different ADL classes, regardless of view, are treated as negatives. This design enforces both cross-view alignment and class-level cohesion, while ensuring separation between different activities.

Contrastive Objective. Let $P_S(i)$ and $P_I(i)$ denote the intra-view and cross-view positive sets for anchor i , and let $A(i)$ denote the set of all non-anchor embeddings in the batch. The instance-level loss is defined as:

$$\mathcal{L}_{\text{SICA},i} = \frac{-1}{|P_S(i)| + |P_I(i)|} \left(\sum_{p \in P_S(i)} \log \frac{\exp(\langle \mathbf{z}_i, \mathbf{z}_p \rangle / \tau)}{\sum_{a \in A(i)} \exp(\langle \mathbf{z}_i, \mathbf{z}_a \rangle / \tau)} + \sum_{p \in P_I(i)} \log \frac{\exp(\langle \mathbf{z}_i, \mathbf{z}_p \rangle / \tau)}{\sum_{a \in A(i)} \exp(\langle \mathbf{z}_i, \mathbf{z}_a \rangle / \tau)} \right), \quad (1)$$

where $\langle \cdot, \cdot \rangle$ denotes cosine similarity and τ is a temperature hyperparameter. The overall batch loss is

$$\mathcal{L}_{\text{SICA}} = \frac{1}{2|B|} \sum_i \mathcal{L}_{\text{SICA},i}$$

This formulation enforces that embeddings of the same activity—across both representation views—are closely aligned, while embeddings of different activities remain well separated. By integrating intra- and cross-view positives, SICA achieves cross-view alignment and class-consistent coherence, producing a shared latent space that is both discriminative and robust.

D. CARE: An End-to-End Framework of Contrastive Alignment for ADL Recognition

While SICA achieves representation-level alignment by enforcing intra-class cohesion and cross-view consistency, it

requires a second-stage classifier to be trained on top of the learned embeddings for downstream ADL recognition. Such two-stage pipelines complicate deployment in real-world smart home systems. To overcome this limitation, we propose an end-to-end framework, **CARE (Contrastive Alignment for ADL Recognition)**, which integrates contrastive alignment and classification into a single-stage framework. In CARE, the model not only produces embeddings aligned across representation views but also outputs activity predictions directly, while classification learning simultaneously guides and regularizes representation learning.

Two-Branch Design. CARE consists of two interconnected branches that share the same sequence and image encoders:

- *Contrastive Representation Learning Branch*: This branch implements SICA. Encoders ($Enc_S(\cdot)$, $Enc_I(\cdot)$) produce view-specific features ($\mathbf{r}_i^S, \mathbf{r}_i^I$), which are projected into a shared latent space via lightweight projections ($Proj_S(\cdot)$, $Proj_I(\cdot)$). The SICA loss \mathcal{L}_{SICA} enforces intra-view consistency and cross-view alignment. It is worth to note that both the sequence encoder and image encoder in CARE are modular components that can be flexibly replaced with alternative encoder architectures.
- *Classification Branch*: In parallel, CARE introduces a supervised classification head. The encoder outputs ($\mathbf{r}_i^S, \mathbf{r}_i^I$) are concatenated and passed to an MLP classifier $Clss_I(\cdot)$ that predicts logits \mathbf{c} . The cross-entropy loss is defined as

$$\mathcal{L}_{CE} = -\frac{1}{|B|} \sum_{i=1}^{|B|} y_i \cdot \log(\sigma(Clss_I(concat(\mathbf{r}_i^S, \mathbf{r}_i^I)))),$$

where σ denotes the softmax function and y_i is the one-hot label for sample i . This branch provides task-level supervision and simultaneously regularizes the shared encoders, preventing them from overfitting to view-specific biases.

Joint Objective. CARE jointly optimizes both branches:

$$\mathcal{L}_{CARE} = \beta \mathcal{L}_{SICA} + (1 - \beta) \mathcal{L}_{CE},$$

where $0 \leq \beta \leq 1$ balances cross-view alignment and supervised classification. The classification head not only enables direct prediction but also provides gradients that complement SICA, improving representation discriminability in an end-to-end manner.

Compared to SICA’s two-stage pipeline, CARE unifies representation alignment and classification into a single training objective. This design eliminates the representation–task mismatch, ensures that embeddings are both cross-view coherent and task-oriented, and yields a fully end-to-end system for robust ADL recognition.

IV. EXPERIMENTS

A. Datasets and Experimental Protocol

Datasets. We evaluate on three CASAS datasets—*Milan*, *Cairo*, and *Kyoto7*—collected in realistic smart-home testbeds with bedrooms, bathrooms, kitchens, living rooms, and dining rooms instrumented by ambient sensors (motion, temperature, door), following Cook *et al.* [13]. *Milan* contains 35 sensors, 15 activity categories, and 4,060 recorded activities; *Cairo*

has 34 sensors, 13 categories, and 842 activities; *Kyoto7* includes 71 sensors, 13 categories, and 634 activities. For comparability, we group the original labels into 11 ADLs, consistent with [11].

Data splits. We adopt a stratified 70/30 train/test split by activity class. On the 70% training portion, we run 5-fold cross-validation for hyperparameter tuning, then retrain on the full training split and evaluate on the held-out test split. Each experiment is repeated with 5 random seeds; we report mean \pm std.

Batching and training. Batch size is 64; training runs up to 60 epochs with early stopping on validation F1. No random window sampling is used.

Encoders. The sequence/image encoders in Sec. III-A and Sec. III-B are architecture-agnostic and can be instantiated with any sequence or image backbone. In our experiments, we instantiate them with *LSTM* or *BiLSTM* for the sequence stream and *ResNet18* for the image stream; the corresponding dual-stream variants are denoted **L-Res** and **BiL-Res**.

B. Overall Performance

Baselines. We compare our method against five categories of baselines: (1) *Traditional ML*: Random Forest, SVM; (2) *Sequence-based*: DeepCASAS [26], Embedding FCN [4], TCN [22], GRU [10], 1D-CNN [25], LSTM-CNN [37]; (3) *Image-based*: DCNN [18], GreyDCNN [28], Transformer [14]; (4) *Graph-based*: GraphModel [31]; (5) *Language-inspired*: TDOST [34], which frames activity recognition under a language modeling paradigm. This diverse set of baselines covers traditional feature-based classifiers, sequence/image/graph encoders, and recent language-inspired models, providing a comprehensive benchmark for evaluating our framework. All baseline and proposed models are trained and evaluated under the *exact same* train/test splits and evaluation protocol, ensuring fairness and eliminating confounding factors due to differing data partitions.

Overall performance. Table II compares all approaches on *Milan*, *Cairo*, and *Kyoto7*. Traditional machine learning models, such as Random Forest and SVM, perform significantly worse than deep learning baselines, underscoring the necessity of representation learning in complex ADL dynamics. Deep learning approaches yield substantially higher performance. Sequence-based baselines (e.g., DeepCASAS, EmbeddingFCN, GRU, LSTM-CNN) achieve competitive results as they usually capture temporal dependencies effectively, but are sometimes more affected by noise and sparsity. While image-based baselines (e.g., BinaryCNN, DCNN, GreyDCNN, Transformer) are generally more robust but may degrade on highly sparse datasets such as *Kyoto7*. This complementarity highlights the importance of integrating both views. The graph-based model performs competitively on *Milan* and *Cairo* by explicitly modeling sensor relationships, but suffers a marked performance degradation on the sparse and noisy *Kyoto7*. By using a textual encoding method, the accuracy of TDOST is generally better than that of all the other baselines except ours, demonstrating the advantage of textual information in

TABLE II: Benchmarking on *Milan*, *Cairo*, and *Kyoto7* (mean \pm std over 5 runs). Time per batch measured on our setup.

Model	Milan				Cairo				Kyoto7				Time/Batch (s)
	Acc.	Prec.	Rec.	F1	Acc.	Prec.	Rec.	F1	Acc.	Prec.	Rec.	F1	
Random Forest	32.0 \pm 9.6	40.0 \pm 4.4	37.8 \pm 6.2	34.8 \pm 4.9	61.7 \pm 9.8	53.9 \pm 9.4	57.4 \pm 5.5	52.6 \pm 5.4	43.2 \pm 4.5	46.8 \pm 5.6	44.6 \pm 3.8	41.4 \pm 4.3	\ll 0.001
SVM	51.1 \pm 1.5	46.1 \pm 1.0	51.1 \pm 1.5	47.6 \pm 1.4	60.0 \pm 2.0	61.3 \pm 2.5	60.0 \pm 2.0	60.1 \pm 2.0	37.0 \pm 2.6	35.9 \pm 4.3	37.0 \pm 2.6	35.8 \pm 3.5	\ll 0.001
DeepCASAS [26]	85.3 \pm 0.8	84.7 \pm 1.6	85.3 \pm 0.8	84.8 \pm 1.2	80.2 \pm 2.4	78.8 \pm 3.4	80.2 \pm 2.4	78.9 \pm 2.8	62.3 \pm 3.2	62.5 \pm 4.2	62.3 \pm 3.2	60.3 \pm 4.0	0.001
JointTemporalModel [19]	78.9 \pm 1.1	75.8 \pm 1.8	78.9 \pm 1.1	77.0 \pm 1.5	77.5 \pm 1.6	80.4 \pm 1.4	77.5 \pm 1.6	78.0 \pm 1.6	59.7 \pm 3.7	60.6 \pm 2.4	59.7 \pm 3.7	58.4 \pm 4.3	0.001
EmbeddingFCN [4]	72.8 \pm 1.6	72.0 \pm 1.5	73.0 \pm 1.4	71.0 \pm 1.6	48.3 \pm 3.5	37.1 \pm 3.3	48.1 \pm 3.4	40.0 \pm 3.4	59.3 \pm 2.0	57.1 \pm 2.0	59.0 \pm 2.1	55.5 \pm 2.2	0.005
TCN [22]	62.2 \pm 0.6	59.5 \pm 1.6	62.2 \pm 0.6	59.4 \pm 0.3	66.8 \pm 2.1	67.6 \pm 2.6	66.8 \pm 2.1	65.3 \pm 3.1	44.2 \pm 0.7	32.4 \pm 0.9	44.2 \pm 0.7	33.7 \pm 2.0	0.003
GRU [10]	76.9 \pm 0.7	75.5 \pm 0.4	76.8 \pm 0.7	75.7 \pm 0.7	83.0 \pm 0.0	82.3 \pm 0.5	82.7 \pm 0.5	82.2 \pm 0.0	63.1 \pm 5.2	63.7 \pm 4.7	63.1 \pm 5.2	60.9 \pm 7.4	0.001
1D-CNN [25]	46.2 \pm 2.2	44.0 \pm 2.8	46.2 \pm 2.2	44.5 \pm 2.4	56.7 \pm 3.3	57.7 \pm 2.5	56.7 \pm 3.3	56.8 \pm 3.2	42.7 \pm 3.4	40.4 \pm 5.1	42.7 \pm 3.4	40.6 \pm 4.3	0.001
LSTM-CNN [37]	71.2 \pm 5.7	67.6 \pm 5.8	71.2 \pm 5.7	69.0 \pm 5.8	62.3 \pm 1.1	56.9 \pm 3.8	62.3 \pm 1.1	58.5 \pm 1.0	50.8 \pm 2.1	51.5 \pm 1.9	50.8 \pm 2.1	45.2 \pm 4.5	0.003
BinaryCNN [35]	79.0 \pm 0.1	78.4 \pm 0.4	79.0 \pm 0.1	78.4 \pm 0.1	82.3 \pm 1.0	83.9 \pm 0.2	82.3 \pm 1.0	82.6 \pm 1.0	66.8 \pm 0.9	70.1 \pm 1.5	66.8 \pm 0.9	66.6 \pm 1.0	0.003
DCNN [18]	81.0 \pm 1.6	80.9 \pm 1.5	81.0 \pm 1.5	80.9 \pm 1.6	75.7 \pm 0.6	77.8 \pm 0.8	75.7 \pm 0.8	76.3 \pm 0.7	72.3 \pm 2.1	72.7 \pm 2.3	72.3 \pm 2.1	73.9 \pm 2.2	0.009
GreyDCNN [28]	68.6 \pm 1.1	68.3 \pm 1.0	68.6 \pm 1.1	67.0 \pm 1.1	80.2 \pm 1.2	81.5 \pm 1.4	80.2 \pm 1.2	79.7 \pm 0.5	68.0 \pm 2.8	66.3 \pm 4.0	68.0 \pm 2.8	66.7 \pm 3.4	0.009
Transformer [14]	77.8 \pm 0.6	74.9 \pm 0.9	77.8 \pm 0.6	75.6 \pm 1.0	71.7 \pm 1.3	71.4 \pm 1.5	71.6 \pm 1.6	70.8 \pm 1.8	56.1 \pm 0.0	58.7 \pm 4.4	56.1 \pm 0.0	56.1 \pm 2.3	0.007
GraphModel [31]	82.8 \pm 0.5	82.3 \pm 0.2	82.8 \pm 0.5	82.3 \pm 0.3	76.7 \pm 0.5	77.1 \pm 0.3	76.7 \pm 0.2	76.8 \pm 0.5	53.4 \pm 1.2	54.2 \pm 1.0	53.4 \pm 1.0	52.0 \pm 1.2	1.586
TDOST [34]	88.7 \pm 1.0	88.5 \pm 0.9	88.7 \pm 1.0	88.4 \pm 0.9	81.0 \pm 0.9	80.3 \pm 1.9	81.0 \pm 0.9	79.3 \pm 1.9	70.0 \pm 1.2	70.0 \pm 1.1	70.0 \pm 1.2	70.0 \pm 1.1	0.001
SICA_{L-Res}	89.8\pm0.3	89.8\pm0.2	89.8\pm0.3	89.6\pm0.2	88.5\pm0.7	89.3\pm0.5	88.5\pm0.7	88.6\pm0.6	72.6\pm1.8	73.9\pm2.4	72.6\pm1.8	72.4\pm1.7	0.010
SICA_{BiL-Res}	89.5\pm0.6	89.7\pm0.5	89.5\pm0.6	89.5\pm0.5	88.9\pm1.3	88.8\pm1.9	88.7\pm1.6	73.3\pm2.6	74.9\pm1.7	73.8\pm2.5	73.3\pm2.6	73.3\pm2.6	0.011

capturing cross-view information. Overall, our SICA models consistently deliver superior performance across all datasets and metrics, establishing a new state of the art.

Computation considerations. In general, image-based models require more computation than sequence-based ones due to the inherent differences in input size and model complexity. GraphModel further exacerbates this with prohibitively high inference time (1.586 s/batch). TDOST consumes only 0.001 seconds per batch by using BiLSTM to inference. Despite leveraging both representation views, our SICA models remain efficient (0.010–0.011 s/batch), on par with image-based baselines and an order of magnitude faster than GraphModel. This favorable trade-off between accuracy and efficiency underscores the scalability of SICA for real-world smart-home ADL recognition.

C. Uni- vs. Within- and Cross-View Alignment

In our supervised contrastive learning framework, we consider two types of positive pairs: (1) *intra-view* pairs, i.e., embeddings from the same view and class (sequence–sequence or image–image); and (2) *cross-view* pairs, i.e., embeddings across views but from the same class. The latter includes both the direct sequence–image pair of the same sample (z_i^S, z_i^I) and cross-sample pairs from the same class (z_i^S, z_j^I with $y_j = y_i$).

We evaluate three variants: (i) **uni-view baselines** (LSTM, BiLSTM, ResNet18), which learn within a single domain; (ii) **within-view alignment**, which applies contrastive loss only to intra-view pairs; and (iii) **cross-view alignment** (our full SICA), which leverages both intra- and cross-view pairs.

As shown in Tab. III, cross-view alignment consistently outperforms all baselines. For instance, BiL-Res achieves gains of $\sim 3\%$ on *Milan*, 2% on *Cairo*, and 1% on *Kyoto7* compared with the best unimodal models. Compared to within-view alignment, cross-view alignment further improves accuracy by 1%, confirming the value of explicitly enforcing consistency across heterogeneous views.

Fig. 5 presents *Cairo* as a representative example, providing class-level evidence of our approach. The results show that

TABLE III: Ablation: uni-, within-, and cross-view alignments: performance metrics (mean \pm std) and computational cost in memory (MiB) and time per batch (s).

Metric	Uni-View			Within-View Align		Cross-View Align	
	LSTM	BiLSTM	ResNet18	L-Res	BiL-Res	L-Res	BiL-Res
Milan	Acc.	86.3 \pm 0.8	86.3 \pm 2.1	87.0 \pm 0.8	89.5 \pm 0.3	89.6 \pm 0.7	89.8\pm0.3
	Prec.	86.0 \pm 0.9	86.1 \pm 2.2	86.8 \pm 1.0	89.6 \pm 0.4	89.9 \pm 0.6	89.8\pm0.2
	Rec.	86.2 \pm 0.8	86.3 \pm 2.2	87.0 \pm 0.8	89.5 \pm 0.3	89.6 \pm 0.7	89.8\pm0.3
	F1	85.9 \pm 0.9	86.1 \pm 2.2	86.4 \pm 1.0	89.3 \pm 0.3	89.5 \pm 0.6	89.6\pm0.2
Cairo	Acc.	83.4 \pm 4.1	83.8 \pm 4.3	76.7 \pm 3.8	88.1 \pm 0.4	88.1 \pm 0.4	88.5\pm0.7
	Prec.	84.5 \pm 3.1	85.2 \pm 3.8	81.6 \pm 1.6	87.6 \pm 0.2	88.6 \pm 1.3	89.3\pm0.5
	Rec.	83.9 \pm 4.5	84.5 \pm 4.4	76.7 \pm 3.8	88.1 \pm 0.4	88.1 \pm 0.4	88.5\pm0.7
	F1	82.3 \pm 6.1	84.1 \pm 4.5	77.4 \pm 3.5	87.8 \pm 0.2	88.1 \pm 0.7	88.6\pm0.6
Kyoto7	Acc.	71.4 \pm 4.0	72.4 \pm 2.7	71.7 \pm 2.7	72.5 \pm 1.3	72.0 \pm 2.9	72.6\pm1.8
	Prec.	72.0 \pm 6.0	72.2 \pm 2.2	70.6 \pm 3.2	72.9 \pm 1.6	73.5 \pm 2.3	73.9\pm2.4
	Rec.	72.0 \pm 4.0	72.2 \pm 2.2	71.7 \pm 2.7	72.5 \pm 1.3	72.0 \pm 3.0	72.6\pm1.8
	F1	71.0 \pm 4.0	71.1 \pm 2.2	71.1 \pm 3.7	71.8 \pm 1.5	72.0 \pm 3.2	72.4\pm1.7
Eff.	Mem.	171.76	313.53	1511.19	1620.17	1716.93	1620.17
	T/B	0.004	0.005	0.006	0.010	0.011	0.010

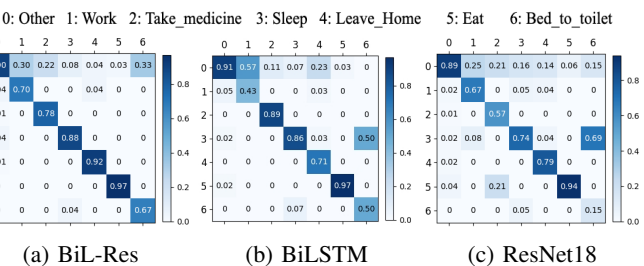


Fig. 5: Heatmap of BiLSTM and ResNet18 on *Cairo*.

SICA leverages the complementary strengths of sequence and image streams: across all activities, it either outperforms both unimodal baselines or matches the stronger one, achieving clear gains on “Work,” “Sleep,” “Leave Home,” and “Bed to toilet,” while remaining competitive on classes such as “Take medicine” and “Eat.” This consistent per-class advantage highlights how cross-view alignment fully exploits complementary temporal and spatial cues, underscoring the robustness of our cross-view approach.

In terms of efficiency, multimodal models require more

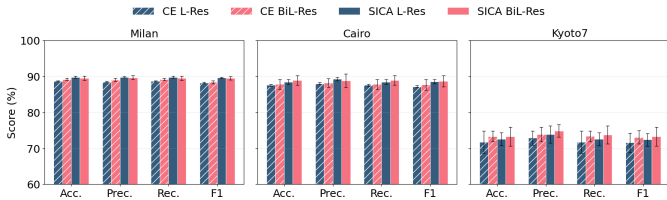


Fig. 6: Ablation: naïve fusion via cross entropy (CE) vs. contrastive alignment (SICA).

memory (e.g., ~ 1.6 GB for ResNet18/SICA vs. 0.17 GB for LSTM), yet their runtime overhead remains modest (0.010–0.011 s/batch), effectively matching ResNet18. This makes the performance–efficiency tradeoff favorable.

D. Contrastive Alignment vs. Naïve Fusion

A natural baseline for multimodal integration is to concatenate the sequence and image embeddings and train with a cross-entropy (CE) loss. While straightforward, this naïve fusion provides no explicit signal to align the two views, leaving the classifier free to overfit to the dominant stream and underutilize complementary cues.

Fig. 6 compares the two approaches across three datasets. SICA have a comparable performance with CE-based fusion, with the largest gains observed on the challenging *Kyoto7* dataset. For example, BiL-Res with SICA improves the F1-score by 1.3% over its CE counterpart. Importantly, these CE models are not previous baselines but architectural counterparts of our framework, differing only in the training objective—underscoring the benefit of contrastive alignment.

The performance gap is most pronounced in *Kyoto7*, which combines limited activity samples (~ 600 instances) with a dense set of 71 sensors, resulting in higher dimension, sparser and noisier inputs compared with the other two datasets. Such conditions hinder naïve concatenation, as the classifier struggles to disentangle redundant activations and overfits view-specific cues. SICA alleviates this by aligning sequence and image representations in a shared latent space, leveraging spatial images to filter redundant activations and enforcing view-invariant, class-consistent features.

Efficiency. Both CE fusion and SICA share the same input and dual-stream encoders, and differ only in the learning objective. As a result, their computational cost is identical, ensuring that SICA’s performance advantage stems from improved representation learning rather than architectural complexity.

Overall, these results confirm that contrastive alignment is not merely an alternative to feature concatenation but a principled mechanism for exploiting cross-view complementarities. By explicitly aligning sequence and image embeddings, SICA yields more robust and generalizable representations, particularly under the data sparsity and noise conditions common in real-world smart home deployments.

E. Temporal Binning and Frequency-based Event Filtering

Temporal binning. We first examine the impact of discretizing timestamps into coarse-grained bins. Fig. 7 reports results

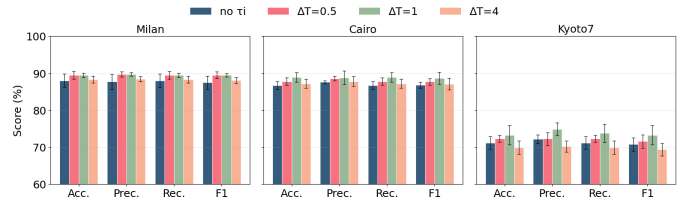


Fig. 7: Performance Comparison Using Different Hour Intervals for Temporal Encoding of BiL-Res.

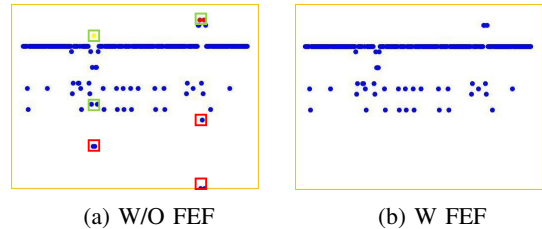


Fig. 8: Event Filtering Example: Eat activity in *Milan*.

with bin widths of 0.5h, 1h, and 4h ($\Delta T \in \{0.5, 1, 4\}$), compared to the case without incorporating time information. The results without incorporating time information is lower than all the other settings by 1–3%, suggesting the importance of timestamps. A 1-hour bin consistently yields the best trade-off across all datasets: finer bins (0.5h) introduce redundancy and unstable variance (e.g., on *Kyoto7*), while coarser bins (4h) discard critical context between adjacent activities. This aligns with the average activity durations (0.25h for *Milan*, 1.09h for *Cairo*, and 0.67h for *Kyoto7*), confirming that the 1-hour setting best balances temporal resolution and robustness.

Frequency-based Event Filtering (FEF). Figure 8 illustrates the effect of FEF on the *Milan* dataset. The filter discards several sensors—shown in red, yellow and some blue—including "M009", "M006" and "M019" in red box (located in the living room and aisle), as well as "M012", "D003" and "T001" in green box (placed in the kitchen). Although FEF eliminates sensors located in the kitchen, which might seem relevant to the "Eat" activity, the triggered frequency of these sensors accounts for less than 7% of the total sensor activations during "Eat". Besides, the accuracy for "Eat" increases from 66.7% to 80.6% by using FEF, indicating that the sensors in the green box are not the most important features for this activity.

Consequently, FEF eliminates sensors that are highly irrelevant to the target activity; however, it may also remove useful information. Therefore, an appropriate filtering threshold must be carefully chosen. We also test the effect of removing sensors with very low activation frequency. As shown in Table IV, the best performance on *Cairo* is achieved with a 1% threshold; results obtained without FEF or at higher thresholds exhibit a slight decline. This suggests that filtering suppresses spurious noise while preserving salient sensor events, with 1% threshold providing the best robustness–information balance.

Together, these ablations confirm that our preprocessing pipeline—hourly temporal binning plus Frequency-based

TABLE IV: BiL-Res on *Cairo*: Frequency-based Event Filtering (FEF) Threshold θ .

θ	Acc.	Prec.	Rec.	F1
W/O FEF	87.0 \pm 2.4	87.2 \pm 2.7	87.0 \pm 2.4	86.7 \pm 2.4
1%	88.9\pm1.3	88.8\pm1.9	88.9\pm1.3	88.7\pm1.6
3%	87.0 \pm 1.8	87.3 \pm 1.6	87.0 \pm 1.8	86.6 \pm 1.9
5%	87.6 \pm 0.5	88.1 \pm 0.3	87.6 \pm 0.5	87.3 \pm 0.7

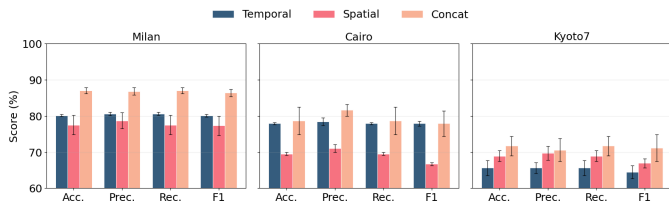


Fig. 9: ResNet18 ablation on image inputs: temporal vs. spatial vs. concatenated.

Event Filtering—strikes the right compromise between noise suppression and information retention, providing a clean foundation for downstream multimodal representation learning.

F. Effectiveness of Image-Based Representations

To interpret the contributions of temporal and spatial cues in image encodings, we train ResNet18 on temporal images, spatial images, and their concatenation. Fig. 9 report the results. Concatenated images consistently outperform single-view inputs, with 5–7% gains on *Milan* and 1–8% on *Cairo*. These results highlight the complementary nature of the two views: temporal images capture fine-grained activity dynamics, while spatial images provide global context via sensor layout and transition statistics. On *Kyoto7*, the gain from concatenation is smaller. This is likely due to its denser sensor deployment and higher noise levels, which make the marginal contribution of explicit spatial images less pronounced. Nevertheless, concatenation never underperforms compared to single views, confirming that temporal–spatial image integration yields more robust and generalizable representations. Crucially, the gains stem from the representation design itself rather than the backbone architecture, underscoring the effectiveness and broad applicability of our image encoding strategy.

To understand the role of different cues, we employ Gradient-weighted Class Activation Mapping (Grad-CAM) [33], a visualization technique that leverages the gradients of a target class flowing into a convolutional layer to generate a heatmap of salient regions for prediction. As shown in Fig. 10, the heatmaps (temporal image on the top and spatial image on the bottom) indicate that temporal images highlight sequential activation patterns, while spatial images emphasize sensor layout regions relevant to transitions. The model distributes its attention across either/both temporal or/and spatial areas, demonstrating that concatenation encourages the network to leverage complementary information sources. This visualization corroborates the quantitative results and explains the consistent performance gains of the joint representation.

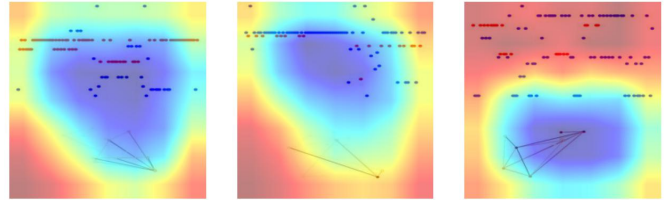


Fig. 10: *Cairo*'s Grad-Cam on Work Activity.

TABLE V: Performance of BiL-Res under sensor corruption and positional perturbations. For corruption settings $a\% \times b\%$, $a\%$ of activity samples are selected and $b\%$ of their sensor events replaced with default values.

Metric	None	Malfunctions and Varying Numbers			Sensor Repositioning			
		5\% \times 5%			$\sigma^2 = 10$	$\sigma^2 = 20$	$\sigma^2 = 30$	
		5\% \times 5%	5\% \times 10%	10\% \times 5%				
Milan	Acc.	89.5\pm0.6	88.3 \pm 1.9	88.3 \pm 1.9	88.3 \pm 1.9	89.7 \pm 2.0	89.7 \pm 2.0	89.5 \pm 1.9
	Prec.	89.7\pm0.5	88.5 \pm 1.9	88.4 \pm 1.9	88.5 \pm 2.0	89.5 \pm 2.1	89.5 \pm 2.1	89.3 \pm 2.0
	Rec.	89.5\pm0.6	88.3 \pm 1.9	88.3 \pm 1.9	88.3 \pm 1.9	89.7 \pm 2.0	89.7 \pm 2.0	89.5 \pm 1.9
	F1	89.5\pm0.5	87.8 \pm 1.9	87.7 \pm 2.0	87.8 \pm 2.0	89.4 \pm 2.1	89.4 \pm 2.1	89.2 \pm 2.0
Cairo	Acc.	88.9\pm1.3	86.6 \pm 1.7	86.4 \pm 1.6	86.2 \pm 1.4	86.3 \pm 1.6	86.3 \pm 1.6	86.3 \pm 1.6
	Prec.	88.8\pm1.9	88.3 \pm 2.1	88.2 \pm 2.0	87.8 \pm 1.8	88.1 \pm 2.1	88.1 \pm 2.1	88.1 \pm 2.1
	Rec.	88.9\pm1.3	86.6 \pm 1.7	86.4 \pm 1.6	86.2 \pm 1.4	86.3 \pm 1.6	86.3 \pm 1.6	86.3 \pm 1.6
	F1	88.7\pm1.6	86.7 \pm 1.8	86.6 \pm 1.7	86.3 \pm 1.5	86.5 \pm 1.7	86.5 \pm 1.7	86.5 \pm 1.7
Kyoto7	Acc.	73.3\pm2.6	73.7 \pm 4.2	74.1 \pm 4.0	73.7 \pm 4.2	73.4 \pm 4.5	73.0 \pm 4.8	73.4 \pm 4.5
	Prec.	74.9\pm1.7	74.1 \pm 4.1	74.6 \pm 3.9	74.1 \pm 4.1	74.1 \pm 3.9	73.9 \pm 4.0	74.1 \pm 3.9
	Rec.	73.8\pm2.5	73.7 \pm 4.2	74.1 \pm 4.0	73.7 \pm 4.2	73.4 \pm 4.5	73.0 \pm 4.8	73.4 \pm 4.5
	F1	73.3\pm2.6	73.1 \pm 4.2	73.5 \pm 3.9	73.1 \pm 4.2	72.8 \pm 4.4	72.5 \pm 4.7	72.8 \pm 4.4

G. Robustness to Sensor Corruption and Layout Variability

In real-world deployments, sensor malfunctions, missing signals, and changes in sensor placement are inevitable sources of distribution shift. To evaluate robustness under such conditions, we test our models trained on clean data directly on corrupted test sets *without retraining*.

Experimental setup. We consider two common types of corruption: (i) *Sensor malfunctions*, where a fraction of activity samples are randomly selected and a percentage of their events are replaced with default values (“OFF,” “CLOSE,” “ABSENT”) to simulate faulty or missing sensors. (ii) *Sensor repositioning*, where sensor coordinates in spatial images are perturbed by Gaussian noise with variance $\sigma^2 \in \{10, 20, 30\}$, mimicking layout changes or misalignments.

Results. As shown in Tab. V, our BiL-Res model exhibits strong resilience: accuracy on *Milan*, *Cairo* and *Kyoto7* drops by only 1–3% across all corruption settings.

We believe the robustness arises from three factors: (1) our preprocessing pipeline filters unstable signals and low-activation sensors, suppressing noise before encoding; (2) the dual-branch sequence–image architecture provides redundancy, allowing one representation view to compensate when the other is degraded; and (3) the SICA loss enforces consistency across views and samples, acting as a strong regularizer against distribution shifts.

V. CONCLUSION

In this paper, we presented CARE, a unified framework that bridges the gap between sequence- and image-based encodings for event-triggered sensor data. Our results demonstrate

that explicitly aligning temporal and spatial cues through supervised contrastive learning not only advances performance beyond unimodal and naïve fusion baselines but also improves robustness to common real-world challenges such as sensor failures and layout variability. Importantly, CARE achieves this with a one-stage joint training strategy, making it more deployment-ready than multi-stage pipelines.

Beyond state-of-the-art performance, our findings highlight a broader insight: temporal and spatial representations are not merely complementary but mutually reinforcing when aligned in a shared latent space. This opens promising directions for generalizing contrastive alignment to other multimodal sensing domains (e.g., combining audio, physiological, or textual streams) and for developing adaptive mechanisms that handle evolving sensor infrastructures in long-term smart home deployments. By providing both methodological advances and practical robustness, CARE represents a step toward more reliable and scalable ambient intelligence systems.

REFERENCES

- [1] Giovanni Acampora, Diane J Cook, Parisa Rashidi, and Athanasios V Vasilakos. A survey on ambient intelligence in healthcare. *Proceedings of the IEEE*, 101(12):2470–2494, 2013.
- [2] Luca Arrotta, Gabriele Civitarese, and Claudio Bettini. Dexar: Deep explainable sensor-based activity recognition in smart-home environments. *Proceedings of the ACM on Interactive, Mobile, Wearable and Ubiquitous Technologies*, 6(1):1–30, 2022.
- [3] Prabakaran Balasubramanian, Vikram Kaushik, Sumaya Y Altamimi, Marco Amabili, and Mohamed Alteneiji. Comparison of neural networks based on accuracy and robustness in identifying impact location for structural health monitoring applications. *Structural Health Monitoring*, 22(1):417–432, 2023.
- [4] Damien Bouchabou, Sao Mai Nguyen, Christophe Lohr, Benoit Leduc, and Ioannis Kanellos. Fully convolutional network bootstrapped by word encoding and embedding for activity recognition in smart homes. In *Deep Learning for Human Activity Recognition: Second International Workshop, DL-HAR 2020, Held in Conjunction with IJCAI-PRICAI 2020, Kyoto, Japan, January 8, 2021, Proceedings 2*, pages 111–125. Springer, 2021.
- [5] Hui Chen, Charles Gouin-Vallerand, Kévin Bouchard, Sébastien Gaboury, Mélanie Couture, Nathalie Bier, and Sylvain Giroux. Contrastive self-supervised learning for sensor-based human activity recognition: A review. *IEEE Access*, 2024.
- [6] Hui Chen, Charles Gouin-Vallerand, Kévin Bouchard, Sébastien Gaboury, Mélanie Couture, Nathalie Bier, and Sylvain Giroux. Enhancing human activity recognition in smart homes with self-supervised learning and self-attention. *Sensors*, 24(3):884, 2024.
- [7] Hui Chen, Charles Gouin-Vallerand, Kévin Bouchard, Sébastien Gaboury, Hubert Kenfack Ngankam, Maxime Lussier, Mélanie Couture, Nathalie Bier, and Sylvain Giroux. Utilizing self-supervised learning for recognizing human activity in older adults through labeling applications in real-world smart homes. In *Proceedings of the 2024 International Conference on Information Technology for Social Good*, pages 275–283, 2024.
- [8] Ting Chen, Simon Kornblith, Mohammad Norouzi, and Geoffrey Hinton. A simple framework for contrastive learning of visual representations. In *International conference on machine learning*, pages 1597–1607. PMLR, 2020.
- [9] Sumit Chopra, Raia Hadsell, and Yann LeCun. Learning a similarity metric discriminatively, with application to face verification. In *2005 IEEE computer society conference on computer vision and pattern recognition (CVPR'05)*, volume 1, pages 539–546. IEEE, 2005.
- [10] Junyoung Chung, Çağlar Gülcöhre, KyungHyun Cho, and Yoshua Bengio. Empirical evaluation of gated recurrent neural networks on sequence modeling. *CoRR*, abs/1412.3555, 2014.
- [11] Diane J Cook. Learning setting-generalized activity models for smart spaces. *IEEE intelligent systems*, 2010(99):1, 2010.
- [12] Diane J Cook, Aaron S Crandall, Brian L Thomas, and Narayanan C Krishnan. Casas: A smart home in a box. *Computer*, 46(7):62–69, 2012.
- [13] Diane J Cook and Maureen Schmitter-Edgecombe. Assessing the quality of activities in a smart environment. *Methods of information in medicine*, 48(05):480–485, 2009.
- [14] Alexey Dosovitskiy, Lucas Beyer, Alexander Kolesnikov, Dirk Weissenborn, Xiaohua Zhai, Thomas Unterthiner, Mostafa Dehghani, Matthias Minderer, Georg Heigold, Sylvain Gelly, Jakob Uszkoreit, and Neil Houlsby. An image is worth 16x16 words: Transformers for image recognition at scale. *CoRR*, abs/2010.11929, 2020.
- [15] Rob Dunne, Tim Morris, and Simon Harper. A survey of ambient intelligence. *ACM Computing Surveys (CSUR)*, 54(4):1–27, 2021.
- [16] Euronews. A third of nurses report witnessing patients die due to staff shortages, new global survey finds. <https://www.euronews.com/health/2023/10/13/a-third-of-nurses-report-witnessing-patients-die-due-to-staff-shortages-new-global-survey-finds>. Accessed: 2024-03-06.
- [17] Arindam Ghosh, Amartya Chakraborty, Dhruv Chakraborty, Mousumi Saha, and Sujoy Saha. Ultrasense: A non-intrusive approach for human activity identification using heterogeneous ultrasonic sensor grid for smart home environment. *Journal of Ambient Intelligence and Humanized Computing*, pages 1–22, 2023.
- [18] Munkhjargal Gochoo, Tan-Hsu Tan, Shing-Hong Liu, Fu-Rong Jean, Fady S Alnajjar, and Shih-Chia Huang. Unobtrusive activity recognition of elderly people living alone using anonymous binary sensors and dnn. *IEEE journal of biomedical and health informatics*, 23(2):693–702, 2018.
- [19] Rebeen Ali Hamad, Longzhi Yang, Wai Lok Woo, and Bo Wei. Joint learning of temporal models to handle imbalanced data for human activity recognition. *Applied Sciences*, 10(15), 2020.
- [20] Shruthi K Hiremath, Yasutaka Nishimura, Sonia Chernova, and Thomas Pötzl. Bootstrapping human activity recognition systems for smart homes from scratch. *Proceedings of the ACM on Interactive, Mobile, Wearable and Ubiquitous Technologies*, 6(3):1–27, 2022.
- [21] HM Sajjad Hossain, MD Abdullah Al Haiz Khan, and Nirmalya Roy. Deactive: scaling activity recognition with active deep learning. *Proceedings of the ACM on Interactive, Mobile, Wearable and Ubiquitous Technologies*, 2(2):1–23, 2018.
- [22] Rui Hu, Bruno Michel, Dario Russo, Niccolò Mora, Guido Matrella, Paolo Ciampolini, Francesca Cocchi, Enrico Montanari, Stefano Nunziata, and Thomas Brunschwiler. An unsupervised behavioral modeling and alerting system based on passive sensing for elderly care. *Future Internet*, 13(1):6, 2020.
- [23] Victor Jüttner, Arthur Fleig, and Erik Buchmann. Chatanalysis revisited: can chatgpt undermine privacy in smart homes with data analysis? *i-com*, 24(1):173–187, 2025.
- [24] Prannay Khosla, Piotr Teterwak, Chen Wang, Aaron Sarna, Yonglong Tian, Phillip Isola, Aaron Maschinot, Ce Liu, and Dilip Krishnan. Supervised contrastive learning. *Advances in neural information processing systems*, 33:18661–18673, 2020.
- [25] Serkan Kiranyaz, Onur Avci, Osama Abdeljaber, Turker Ince, Moncef Gabbouj, and Daniel J. Inman. 1d convolutional neural networks and applications: A survey. *Mechanical Systems and Signal Processing*, 151:107398, 2021.
- [26] Daniele Licitetti, Michele Bernardini, Luca Romeo, and Emanuele Fronzoni. A sequential deep learning application for recognising human activities in smart homes. *Neurocomputing*, 396:501–513, 2020.
- [27] T Manoj and GS Thyagaraju. Active and assisted living: A comprehensive review of enabling technologies and scenarios. *International Journal of Advanced Research in Computer Science*, 9(1), 2018.
- [28] Gadelhag Mohamed, Ahmad Lotfi, and Amir Pourabdollah. Employing a deep convolutional neural network for human activity recognition based on binary ambient sensor data. In *Proceedings of the 13th ACM international conference on pervasive technologies related to assistive environments*, pages 1–7, 2020.
- [29] George A Oguntala, Yim Fun Hu, Ali AS Alabdullah, Raed A Abd-Alhameed, Muhammad Ali, and Doanh K Luong. Passive rfid module with lstm recurrent neural network activity classification algorithm for ambient-assisted living. *IEEE Internet of Things Journal*, 8(13):10953–10962, 2021.
- [30] World Health Organization. Ageing and health. <https://www.who.int/news-room/fact-sheets/detail/ageing-and-health>, 2022. Accessed: 2024-08-08.

- [31] Srivatsa P and Thomas Plötz. Using graphs to perform effective sensor-based human activity recognition in smart homes. *Sensors*, 24(12), 2024.
- [32] Martin Prince, Renata Bryce, Emiliano Albanese, Anders Wimo, Wagner Ribeiro, and Cleusa P Ferri. The global prevalence of dementia: a systematic review and metaanalysis. *Alzheimer's & dementia*, 9(1):63–75, 2013.
- [33] Ramprasaath R Selvaraju, Michael Cogswell, Abhishek Das, Ramakrishna Vedantam, Devi Parikh, and Dhruv Batra. Grad-cam: Visual explanations from deep networks via gradient-based localization. In *Proceedings of the IEEE international conference on computer vision*, pages 618–626, 2017.
- [34] Megha Thukral, Sourish Gunesh Dhekane, Shruthi K. Hiremath, Harish Haresamudram, and Thomas Ploetz. Layout-agnostic human activity recognition in smart homes through textual descriptions of sensor triggers (tdost). *Proc. ACM Interact. Mob. Wearable Ubiquitous Technol.*, 9(1), March 2025.
- [35] Aiguo Wang, Shenghui Zhao, Chundi Zheng, Jing Yang, Guilin Chen, and Chih-Yung Chang. Activities of daily living recognition with binary environment sensors using deep learning: A comparative study. *IEEE Sensors Journal*, 21(4):5423–5433, 2021.
- [36] Alyssa Weakley and Maureen Schmitter-Edgecombe. Naturalistic assessment of task interruption in individuals with mild cognitive impairment. *Neuropsychology*, 33(1):1, 2019.
- [37] Kun Xia, Jianguang Huang, and Hanyu Wang. Lstm-cnn architecture for human activity recognition. *IEEE Access*, 8:56855–56866, 2020.